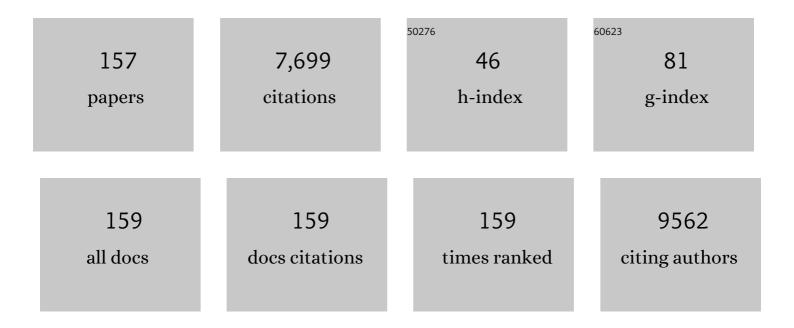
Heinz-Peter Schlemmer

List of Publications by Year in descending order

Source: https://exaly.com/author-pdf/6841159/publications.pdf Version: 2024-02-01



#	Article	IF	CITATIONS
1	Radiomic Profiling of Glioblastoma: Identifying an Imaging Predictor of Patient Survival with Improved Performance over Established Clinical and Radiologic Risk Models. Radiology, 2016, 280, 880-889.	7.3	345
2	Automated brain extraction of multisequence MRI using artificial neural networks. Human Brain Mapping, 2019, 40, 4952-4964.	3.6	284
3	Automated quantitative tumour response assessment of MRI in neuro-oncology with artificial neural networks: a multicentre, retrospective study. Lancet Oncology, The, 2019, 20, 728-740.	10.7	271
4	Multiparametric Magnetic Resonance Imaging (MRI) and MRI–Transrectal Ultrasound Fusion Biopsy for Index Tumor Detection: Correlation with Radical Prostatectomy Specimen. European Urology, 2016, 70, 846-853.	1.9	258
5	Radiogenomics of Glioblastoma: Machine Learning–based Classification of Molecular Characteristics by Using Multiparametric and Multiregional MR Imaging Features. Radiology, 2016, 281, 907-918.	7.3	236
6	Large-scale Radiomic Profiling of Recurrent Glioblastoma Identifies an Imaging Predictor for Stratifying Anti-Angiogenic Treatment Response. Clinical Cancer Research, 2016, 22, 5765-5771.	7.0	230
7	Classification of Cancer at Prostate MRI: Deep Learning versus Clinical PI-RADS Assessment. Radiology, 2019, 293, 607-617.	7.3	214
8	Guidelines for Acquisition, Interpretation, and Reporting of Whole-Body MRI in Myeloma: Myeloma Response Assessment and Diagnosis System (MY-RADS). Radiology, 2019, 291, 5-13.	7.3	209
9	Comparative Analysis of Transperineal Template Saturation Prostate Biopsy Versus Magnetic Resonance Imaging Targeted Biopsy with Magnetic Resonance Imaging-Ultrasound Fusion Guidance. Journal of Urology, 2015, 193, 87-94.	0.4	196
10	The Value of PSA Density in Combination with PI-RADSâ,,¢ for the Accuracy of Prostate Cancer Prediction. Journal of Urology, 2017, 198, 575-582.	0.4	179
11	Radiomic subtyping improves disease stratification beyond key molecular, clinical, and standard imaging characteristics in patients with glioblastoma. Neuro-Oncology, 2018, 20, 848-857.	1.2	170
12	Relaxation-compensated CEST-MRI of the human brain at 7 T: Unbiased insight into NOE and amide signal changes in human glioblastoma. NeuroImage, 2015, 112, 180-188.	4.2	165
13	Radiomic Machine Learning for Characterization of Prostate Lesions with MRI: Comparison to ADC Values. Radiology, 2018, 289, 128-137.	7.3	162
14	Can pre-operative contrast-enhanced dynamic MR imaging for prostate cancer predict microvessel density in prostatectomy specimens?. European Radiology, 2004, 14, 309-317.	4.5	156
15	Comparison of hybrid 68Ga-PSMA PET/MRI and 68Ga-PSMA PET/CT in the evaluation of lymph node and bone metastases of prostate cancer. European Journal of Nuclear Medicine and Molecular Imaging, 2016, 43, 70-83.	6.4	148
16	Combined Clinical Parameters and Multiparametric Magnetic Resonance Imaging for Advanced Risk Modeling of Prostate Cancer—Patient-tailored Risk Stratification Can Reduce Unnecessary Biopsies. European Urology, 2017, 72, 888-896.	1.9	136
17	Definitions of terms, processes and a minimum dataset for transperineal prostate biopsies: a standardization approach of the <scp>G</scp> insburg <scp>S</scp> tudy <scp>G</scp> roup for <scp>E</scp> nhanced <scp>P</scp> rostate <scp>D</scp> iagnostics. BJU International, 2013, 112, 568-577.	2.5	125
18	Local recurrence of prostate cancer after radical prostatectomy is at risk to be missed in 68Ga-PSMA-11-PET of PET/CT and PET/MRI: comparison with mpMRI integrated in simultaneous PET/MRI. European Journal of Nuclear Medicine and Molecular Imaging, 2017, 44, 776-787.	6.4	124

#	Article	IF	CITATIONS
19	Assessing the predictability of <i>IDH</i> mutation and <i>MGMT</i> methylation status in glioma patients using relaxation-compensated multipool CEST MRI at 7.0 T. Neuro-Oncology, 2018, 20, 1661-1671.	1.2	119
20	Fast and Noninvasive Characterization of Suspicious Lesions Detected at Breast Cancer X-Ray Screening: Capability of Diffusion-weighted MR Imaging with MIPs. Radiology, 2016, 278, 689-697.	7.3	113
21	Prediction of malignancy by a radiomic signature from contrast agentâ€free diffusion MRI in suspicious breast lesions found on screening mammography Journal of Magnetic Resonance Imaging, 2017, 46, 604-616.	3.4	113
22	Tumor Infiltration in Enhancing and Non-Enhancing Parts of Glioblastoma: A Correlation with Histopathology. PLoS ONE, 2017, 12, e0169292.	2.5	113
23	Downfieldâ€NOEâ€suppressed amideâ€CESTâ€MRI at 7 Tesla provides a unique contrast in human glioblastoma. Magnetic Resonance in Medicine, 2017, 77, 196-208.	3.0	108
24	Multicentre evaluation of targeted and systematic biopsies using magnetic resonance and ultrasound imageâ€fusion guided transperineal prostate biopsy in patients with a previous negative biopsy. BJU International, 2017, 120, 631-638.	2.5	104
25	No Signal Intensity Increase in the Dentate Nucleus on Unenhanced T1-weighted MR Images after More than 20 Serial Injections of Macrocyclic Gadolinium-based Contrast Agents. Radiology, 2017, 282, 699-707.	7.3	98
26	Can Virtual Contrast Enhancement in Brain MRI Replace Gadolinium?. Investigative Radiology, 2019, 54, 653-660.	6.2	93
27	Pseudoprogression in patients with glioblastoma: clinical relevance despite low incidence. Neuro-Oncology, 2015, 17, 151-159.	1.2	90
28	Relative cerebral blood volume is a potential predictive imaging biomarker of bevacizumab efficacy in recurrent glioblastoma. Neuro-Oncology, 2015, 17, 1139-1147.	1.2	89
29	Radiomics Based on Adapted Diffusion Kurtosis Imaging Helps to Clarify Most Mammographic Findings Suspicious for Cancer. Radiology, 2018, 287, 761-770.	7.3	81
30	Suitable reference tissues for quantitative susceptibility mapping of the brain. Magnetic Resonance in Medicine, 2017, 78, 204-214.	3.0	80
31	Pediatric Brain: No Increased Signal Intensity in the Dentate Nucleus on Unenhanced T1-weighted MR Images after Consecutive Exposure to a Macrocyclic Gadolinium-based Contrast Agent. Radiology, 2017, 283, 828-836.	7.3	74
32	Tlï•weighted Dynamic Glucose-enhanced MR Imaging in the Human Brain. Radiology, 2017, 285, 914-922.	7.3	72
33	Adiabatically prepared spinâ€lock approach for T1Ïâ€based dynamic glucose enhanced MRI at ultrahigh fields. Magnetic Resonance in Medicine, 2017, 78, 215-225.	3.0	71
34	Cadaver-specific CT scans visualized at the dissection table combined with virtual dissection tables improve learning performance in general gross anatomy. European Radiology, 2017, 27, 2153-2160.	4.5	68
35	Relaxation-compensated amide proton transfer (APT) MRI signal intensity is associated with survival and progression in high-grade glioma patients. European Radiology, 2019, 29, 4957-4967.	4.5	64
36	Chemical exchange saturation transfer MRI serves as predictor of early progression in glioblastoma patients. Oncotarget, 2018, 9, 28772-28783.	1.8	63

#	Article	IF	CITATIONS
37	Nuclear Overhauser Enhancement Mediated Chemical Exchange Saturation Transfer Imaging at 7 Tesla in Glioblastoma Patients. PLoS ONE, 2014, 9, e104181.	2.5	62
38	X-ray-Based Techniques to Study the Nano–Bio Interface. ACS Nano, 2021, 15, 3754-3807.	14.6	60
39	Fast and Quantitative T1ï•weighted Dynamic Glucose Enhanced MRI. Scientific Reports, 2017, 7, 42093.	3.3	58
40	Early response assessment of glioma patients to definitive chemoradiotherapy using chemical exchange saturation transfer imaging at 7 T. Journal of Magnetic Resonance Imaging, 2019, 50, 1268-1277.	3.4	58
41	Lung nodule detection in a high-risk population: Comparison of magnetic resonance imaging and low-dose computed tomography. European Journal of Radiology, 2014, 83, 600-605.	2.6	54
42	Potential of quantitative susceptibility mapping for detection of prostatic calcifications. Journal of Magnetic Resonance Imaging, 2017, 45, 889-898.	3.4	54
43	Investigation of the halo-artifact in 68Ga-PSMA-11-PET/MRI. PLoS ONE, 2017, 12, e0183329.	2.5	53
44	Advanced abdominal imaging with dual energy CT is feasible without increasing radiation dose. Cancer Imaging, 2016, 16, 15.	2.8	52
45	MR Perfusion–derived Hemodynamic Parametric Response Mapping of Bevacizumab Efficacy in Recurrent Glioblastoma. Radiology, 2016, 279, 542-552.	7.3	51
46	Acute Toxicity and Quality of Life in Patients With Prostate Cancer Treated With Protons or Carbon Ions in a Prospective Randomized Phase II Study—The IPI Trial. International Journal of Radiation Oncology Biology Physics, 2016, 95, 435-443.	0.8	49
47	Relaxationâ€compensated APT and rNOE CESTâ€MRI of human brain tumors at 3 T. Magnetic Resonance in Medicine, 2019, 82, 622-632.	3.0	49
48	Asymmetry of Deep Medullary Veins on Susceptibility Weighted MRI in Patients with Acute MCA Stroke Is Associated with Poor Outcome. PLoS ONE, 2015, 10, e0120801.	2.5	49
49	Prospective comparison of transperineal magnetic resonance imaging/ultrasonography fusion biopsy and transrectal systematic biopsy in biopsyâ€naÃīve patients. BJU International, 2018, 121, 53-60.	2.5	47
50	Application of (18)F-FDG PET and diffusion weighted imaging (DWI) in multiple myeloma: comparison of functional imaging modalities. American Journal of Nuclear Medicine and Molecular Imaging, 2015, 5, 479-92.	1.0	45
51	Comparison of (18)F-FDG PET/CT and PET/MRI in patients with multiple myeloma. American Journal of Nuclear Medicine and Molecular Imaging, 2015, 5, 469-78.	1.0	44
52	Independent value of image fusion in unenhanced breast MRI using diffusion-weighted and morphological T2-weighted images for lesion characterization in patients with recently detected BI-RADS 4/5 x-ray mammography findings. European Radiology, 2017, 27, 562-569.	4.5	40
53	Differentiation of pseudoprogression and real progression in glioblastoma using ADC parametric response maps. PLoS ONE, 2017, 12, e0174620.	2.5	39
54	Combined Clinical Parameters and Multiparametric Magnetic Resonance Imaging for the Prediction of Extraprostatic Disease—A Risk Model for Patient-tailored Risk Stratification When Planning Radical Prostatectomy. European Urology Focus, 2020, 6, 1205-1212.	3.1	39

#	Article	IF	CITATIONS
55	Joint Imaging Platform for Federated Clinical Data Analytics. JCO Clinical Cancer Informatics, 2020, 4, 1027-1038.	2.1	39
56	Quantitative Dynamic Oxygen 17 MRI at 7.0 T for the Cerebral Oxygen Metabolism in Glioma. Radiology, 2020, 295, 181-189.	7.3	37
57	Nuclear Overhauser Enhancement Imaging of Glioblastoma at 7 Tesla: Region Specific Correlation with Apparent Diffusion Coefficient and Histology. PLoS ONE, 2015, 10, e0121220.	2.5	36
58	Clinical parameters outweigh diffusion- and perfusion-derived MRI parameters in predicting survival in newly diagnosed glioblastoma. Neuro-Oncology, 2016, 18, 1673-1679.	1.2	36
59	Voxel-wise radiogenomic mapping of tumor location with key molecular alterations in patients with glioma. Neuro-Oncology, 2018, 20, 1517-1524.	1.2	36
60	Automatic Analysis of Cellularity in Glioblastoma and Correlation with ADC Using Trajectory Analysis and Automatic Nuclei Counting. PLoS ONE, 2016, 11, e0160250.	2.5	35
61	Volumetric mapping of intra―and extracellular pH in the human brain using ³¹ P MRSI at 7T. Magnetic Resonance in Medicine, 2020, 84, 1707-1723.	3.0	34
62	The Value of Prostate-specific Antigen Density for Prostate Imaging-Reporting and Data System 3 Lesions on Multiparametric Magnetic Resonance Imaging: A Strategy to Avoid Unnecessary Prostate Biopsies. European Urology Focus, 2021, 7, 325-331.	3.1	34
63	The Impact of Magnetic Resonance Imaging on Prediction of Extraprostatic Extension and Prostatectomy Outcome in Patients with Low-, Intermediate- and High-Risk Prostate Cancer: Try to Find a Standard. Journal of Endourology, 2015, 29, 1396-1405.	2.1	32
64	Assessment of tumor oxygenation and its impact on treatment response in bevacizumab-treated recurrent glioblastoma. Journal of Cerebral Blood Flow and Metabolism, 2017, 37, 485-494.	4.3	32
65	Simultaneous whole-body 18F–PSMA-1007-PET/MRI with integrated high-resolution multiparametric imaging of the prostatic fossa for comprehensive oncological staging of patients with prostate cancer: a pilot study. European Journal of Nuclear Medicine and Molecular Imaging, 2018, 45, 340-347.	6.4	32
66	Pose-independent surface matching for intra-operative soft-tissue marker-less registration. Medical Image Analysis, 2014, 18, 1101-1114.	11.6	31
67	Quantification of Tumor Vessels in Glioblastoma Patients Using Time-of-Flight Angiography at 7 Tesla: A Feasibility Study. PLoS ONE, 2014, 9, e110727.	2.5	30
68	A New Approach for Photorealistic Visualization of Rendered Computed TomographyÂlmages. World Neurosurgery, 2018, 114, e283-e292.	1.3	29
69	On a fractional order calculus model in diffusion weighted breast imaging to differentiate between malignant and benign breast lesions detected on X-ray screening mammography. PLoS ONE, 2017, 12, e0176077.	2.5	28
70	Standardized Magnetic Resonance Imaging Reporting Using the Prostate Cancer Radiological Estimation of Change in Sequential Evaluation Criteria and Magnetic Resonance Imaging/Transrectal Ultrasound Fusion with Transperineal Saturation Biopsy to Select Men on Active Surveillance. European Urology Focus, 2021, 7, 102-110.	3.1	28
71	Correlation between genomic index lesions and mpMRI and 68Ga-PSMA-PET/CT imaging features in primary prostate cancer. Scientific Reports, 2018, 8, 16708.	3.3	27
72	Sensitivity of different MRI sequences in the early detection of melanoma brain metastases. PLoS ONE, 2018, 13, e0193946.	2.5	27

#	Article	IF	CITATIONS
73	Chemical exchange saturation transfer (CEST) signal intensity at 7T MRI of WHO IV° gliomas is dependent on the anatomic location. Journal of Magnetic Resonance Imaging, 2019, 49, 777-785.	3.4	27
74	A novel normalization for amide proton transfer CEST MRI to correct for fat signal–induced artifacts: application to human breast cancer imaging. Magnetic Resonance in Medicine, 2020, 83, 920-934.	3.0	26
75	Dorsal root ganglia hypertrophy as in vivo correlate of oxaliplatin-induced polyneuropathy. PLoS ONE, 2017, 12, e0183845.	2.5	26
76	Diffusion-mediated dephasing in the dipole field around a single spherical magnetic object. Magnetic Resonance Imaging, 2015, 33, 1126-1145.	1.8	25
77	Increased microcirculation detected by dynamic contrastâ€enhanced magnetic resonance imaging is of prognostic significance in asymptomatic myeloma. British Journal of Haematology, 2016, 174, 127-135.	2.5	25
78	Multiple Myeloma Guidelines and Their Recent Updates: ImplicationsÂfor Imaging. RoFo Fortschritte Auf Dem Gebiet Der Rontgenstrahlen Und Der Bildgebenden Verfahren, 2019, 191, 998-1009.	1.3	25
79	Improved clinical workflow for simultaneous whole-body PET/MRI using high-resolution CAIPIRINHA-accelerated MR-based attenuation correction. European Journal of Radiology, 2017, 96, 12-20.	2.6	24
80	Histopathological to multiparametric MRI spatial mapping of extended systematic sextant and MR/TRUS-fusion-targeted biopsy of the prostate. European Radiology, 2019, 29, 1820-1830.	4.5	24
81	Simulated clinical deployment of fully automatic deep learning for clinical prostate MRI assessment. European Radiology, 2021, 31, 302-313.	4.5	24
82	7-T ³⁵ Cl and ²³ Na MR Imaging for Detection of Mutation-dependent Alterations in Muscular Edema and Fat Fraction with Sodium and Chloride Concentrations in Muscular Periodic Paralyses. Radiology, 2016, 280, 848-859.	7.3	23
83	The role of perfusion effects in monitoring of chemoradiotherapy of rectal carcinoma using diffusion-weighted imaging. Cancer Imaging, 2013, 13, 548-556.	2.8	22
84	Towards markerless navigation for percutaneous needle insertions. International Journal of Computer Assisted Radiology and Surgery, 2016, 11, 107-117.	2.8	22
85	Ultra-high-field sodium MRI as biomarker for tumor extent, grade and IDH mutation status in glioma patients. NeuroImage: Clinical, 2020, 28, 102427.	2.7	22
86	Relaxation-compensated CEST (chemical exchange saturation transfer) imaging in breast cancer diagnostics at 7T. European Journal of Radiology, 2020, 129, 109068.	2.6	22
87	Repeatability and Reproducibility of ADC Measurements and MRI Signal Intensity Measurements of Bone Marrow in Monoclonal Plasma Cell Disorders. Investigative Radiology, 2022, 57, 272-281.	6.2	22
88	Qualitative and quantitative image analysis of CT and MR imaging in patients with neuroendocrine liver metastases in comparison to 68Ga-DOTATOC PET. European Journal of Radiology, 2015, 84, 1593-1600.	2.6	21
89	Prognostic value of combined visualization of MR diffusion and perfusion maps in glioblastoma. Journal of Neuro-Oncology, 2016, 126, 463-472.	2.9	21
90	Abbreviated MRI Protocols in Breast Cancer Diagnostics. Journal of Magnetic Resonance Imaging, 2019, 49, 647-658.	3.4	21

#	Article	IF	CITATIONS
91	Global Challenges for Cancer Imaging. Journal of Global Oncology, 2018, 4, 1-10.	0.5	20
92	Realâ€ŧime 4DMRIâ€based internal target volume definition for moving lung tumors. Medical Physics, 2020, 47, 1431-1442.	3.0	20
93	Improvement of PI-RADS-dependent prostate cancer classification by quantitative image assessment using radiomics or mean ADC. Magnetic Resonance Imaging, 2021, 82, 9-17.	1.8	19
94	Prognostic significance of tumor burden assessed by whole-body magnetic resonance imaging in multiple myeloma patients treated with allogeneic stem cell transplantation. Haematologica, 2018, 103, 336-343.	3.5	18
95	Vessel architecture imaging using multiband gradient-echo/spin-echo EPI. PLoS ONE, 2019, 14, e0220939.	2.5	18
96	Potential of contrast agents based on highâ€Z elements for contrastâ€enhanced photonâ€counting computed tomography. Medical Physics, 2020, 47, 6179-6190.	3.0	18
97	Comparison of Prostate MRI Lesion Segmentation Agreement Between Multiple Radiologists and a Fully Automatic Deep Learning System. RoFo Fortschritte Auf Dem Gebiet Der Rontgenstrahlen Und Der Bildgebenden Verfahren, 2021, 193, 559-573.	1.3	18
98	Effects of arm truncation on the appearance of the halo artifact in 68Ga-PSMA-11 (HBED-CC) PET/MRI. European Journal of Nuclear Medicine and Molecular Imaging, 2017, 44, 1636-1646.	6.4	17
99	High-resolution FLAIR MRI at 7 Tesla for treatment planning in glioblastoma patients. Radiotherapy and Oncology, 2019, 130, 180-184.	0.6	17
100	Photonâ€counting normalized metal artifact reduction (NMAR) in diagnostic CT. Medical Physics, 2021, 48, 3572-3582.	3.0	17
101	New bone post-processing tools in forensic imaging: a multi-reader feasibility study to evaluate detection time and diagnostic accuracy in rib fracture assessment. International Journal of Legal Medicine, 2017, 131, 489-496.	2.2	15
102	Structured Reporting of Solid and Cystic Pancreatic Lesions in CT and MRI: Consensus-Based Structured Report Templates of the German Society of Radiology (DRG). RoFo Fortschritte Auf Dem Gebiet Der Rontgenstrahlen Und Der Bildgebenden Verfahren, 2020, 192, 641-656.	1.3	15
103	Clinical routine acquisition protocol for 3D relaxationâ€compensated APT and rNOE CESTâ€MRI of the human brain at 3T. Magnetic Resonance in Medicine, 2021, 86, 393-404.	3.0	15
104	Evaluation of an Automated Analysis Tool for Prostate Cancer Prediction Using Multiparametric Magnetic Resonance Imaging. PLoS ONE, 2016, 11, e0159803.	2.5	14
105	Improved detection of melanoma metastases by iodine maps from dual energy CT. European Journal of Radiology, 2017, 90, 27-33.	2.6	14
106	Sensitive and non-invasive assessment of hepatocellular iron using a novel room-temperature susceptometer. Journal of Hepatology, 2017, 67, 535-542.	3.7	13
107	Prediction of significant prostate cancer in biopsy-naÃ ⁻ ve men: Validation of a novel risk model combining MRI and clinical parameters and comparison to an ERSPC risk calculator and PI-RADS. PLoS ONE, 2019, 14, e0221350.	2.5	13
108	Magnetic resonance imagingâ€guided transurethral ultrasound ablation in patients with localised prostate cancer: 3â€year outcomes of a prospective Phase I study. BJU International, 2021, 127, 544-552.	2.5	13

#	Article	IF	CITATIONS
109	Microstructural Analysis of Peripheral Lung Tissue through CPMG Inter-Echo Time R2 Dispersion. PLoS ONE, 2015, 10, e0141894.	2.5	12
110	Contrast-enhanced cadaver-specific computed tomography in gross anatomy teaching. European Radiology, 2018, 28, 2838-2844.	4.5	11
111	Susceptibility based multiparametric quantification of liver disease: Non-invasive evaluation of steatosis and iron overload. Magnetic Resonance Imaging, 2019, 63, 114-122.	1.8	11
112	Susceptibilityâ€weighted imaging in malignant melanoma brain metastasis. Journal of Magnetic Resonance Imaging, 2019, 50, 1251-1259.	3.4	11
113	Dynamic glucoseâ€enhanced (DCE) MRI in the human brain at 7 T with reduced motionâ€induced artifacts based on quantitative R 1ï•mapping. Magnetic Resonance in Medicine, 2020, 84, 182-191.	3.0	11
114	MR–Consistent Simultaneous Reconstruction of Attenuation and Activity for Non–TOF PET/MR. IEEE Transactions on Nuclear Science, 2016, 63, 2443-2451.	2.0	10
115	Dynamic contrast enhanced MRI monitoring of primary proton and carbon ion irradiation of prostate cancer using a novel hypofractionated raster scan technique. Radiotherapy and Oncology, 2016, 120, 313-319.	0.6	10
116	Ultra-High- <i>b</i> -Value Kurtosis Imaging for Noninvasive Tissue Characterization of Ovarian Lesions. Radiology, 2020, 296, 358-369.	7.3	10
117	Assessment of Melanin Content and its Influence on Susceptibility Contrast in Melanoma Metastases. Clinical Neuroradiology, 2020, 30, 607-614.	1.9	9
118	Mask-Adapted Background Field Removal for Artifact Reduction in Quantitative Susceptibility Mapping of the Prostate. Tomography, 2017, 3, 96-100.	1.8	9
119	Na MRI and myometry to compare eplerenone vs. glucocorticoid treatment in Duchenne dystrophy. Acta Myologica, 2017, 36, 2-13.	1.5	9
120	Diffusionâ€weighted MRI treatment monitoring of primary hypofractionated proton and carbon ion prostate cancer irradiation using raster scan technique. Journal of Magnetic Resonance Imaging, 2017, 46, 850-860.	3.4	8
121	Incidental pulmonary emboli in stage IV melanoma patients: Prevalence in CT staging examinations and improved detection with vessel reconstructions based on dual energy CT. PLoS ONE, 2018, 13, e0199458.	2.5	8
122	Dual-contrast pCASL using simultaneous gradient-echo/spin-echo multiband EPI. Magnetic Resonance Imaging, 2019, 57, 359-367.	1.8	8
123	Analyzing Longitudinal wb-MRI Data and Clinical Course in a Cohort of Former Smoldering Multiple Myeloma Patients: Connections between MRI Findings and Clinical Progression Patterns. Cancers, 2021, 13, 961.	3.7	8
124	Imaging of prostate cancer. Deutsches Ärzteblatt International, 2021, , .	0.9	8
125	Wholeâ€body magnetic resonance imaging plus serological followâ€up for early identification of progression in smouldering myeloma patients to prevent development of endâ€organ damage. British Journal of Haematology, 2022, 199, 65-75.	2.5	8
126	Spatial Distribution of Focal Lesions in Whole-Body MRI and Influence of MRI Protocol on Staging in Patients with Smoldering Multiple Myeloma According to the New SLiM-CRAB-Criteria. Cancers, 2020, 12, 2537.	3.7	7

#	Article	IF	CITATIONS
127	The anterior eye chamber: entry of the natural excretion pathway of gadolinium contrast agents?. European Radiology, 2020, 30, 4633-4640.	4.5	7
128	Radiological Monitoring of Modern Immunotherapy: AÂNovelÂChallenge for Interdisciplinary Patient Care. RoFo Fortschritte Auf Dem Gebiet Der Rontgenstrahlen Und Der Bildgebenden Verfahren, 2020, 192, 235-245.	1.3	7
129	Comparison of single-scanner single-protocol quantitative ADC measurements to ADC ratios to detect clinically significant prostate cancer. European Journal of Radiology, 2021, 136, 109538.	2.6	7
130	Mapping an Extended Metabolic Profile of Gliomas Using High-Resolution 31P MRSI at 7T. Frontiers in Neurology, 2021, 12, 735071.	2.4	7
131	Forensic Imaging for Causal Investigation of Death. Korean Journal of Radiology, 2014, 15, 205.	3.4	6
132	Macroangiopathy is a positive predictive factor for response to immunotherapy. Scientific Reports, 2019, 9, 9728.	3.3	6
133	No Changes in T1 Relaxometry After a Mean of 11 Administrations of Gadobutrol. Investigative Radiology, 2020, 55, 381-386.	6.2	6
134	High-intensity focused ultrasound (HIFU) hemiablation of the prostate: Late follow-up MRI findings in non-recurrent patients. European Journal of Radiology, 2021, 144, 109957.	2.6	6
135	Assessment of Sodium MRI at 7 Tesla as Predictor of Therapy Response and Survival in Glioblastoma Patients. Frontiers in Neuroscience, 2021, 15, 782516.	2.8	6
136	Influence of residual fat signal on diffusion kurtosis MRI of suspicious mammography findings. Scientific Reports, 2020, 10, 13286.	3.3	5
137	Strengths and Weaknesses of Nonâ€enhanced and Contrastâ€enhanced Cadaver Computed Tomography Scans in the Teaching of Gross Anatomy in an Integrated Curriculum. Anatomical Sciences Education, 2021, , .	3.7	5
138	Pre-examinations Improve Automated Metastases Detection on Cranial MRI. Investigative Radiology, 2021, 56, 320-327.	6.2	5
139	Anterior chamber enhancement predicts optic nerve infiltration in retinoblastoma. European Radiology, 2022, 32, 7354-7364.	4.5	5
140	Gibbs point field model quantifies disorder in microvasculature of U87-glioblastoma. Journal of Theoretical Biology, 2020, 494, 110230.	1.7	4
141	Motion correction for threeâ€dimensional chemical exchange saturation transfer imaging without direct water saturation artifacts. NMR in Biomedicine, 2022, 35, e4720.	2.8	4
142	Voxel-size dependent quantitative susceptibility mapping of blood vessel networks: A simulation study. Zeitschrift Fur Medizinische Physik, 2019, 29, 282-291.	1.5	3
143	Impact of Surgeon's Experience in Rigid Versus Elastic MRI/TRUS-Fusion Biopsy to Detect Significant Prostate Cancer Using Targeted and Systematic Cores. Cancers, 2022, 14, 886.	3.7	3
144	Potential of quantitative susceptibility mapping for detection of prostatic calcifications. Journal of Magnetic Resonance Imaging, 2017, 45, spcone.	3.4	2

#	Article	IF	CITATIONS
145	CT- and ultrasound-characteristics of hepatic lesions in patients with multiple endocrine neoplasia syndrome. A retrospective image review of 25 cases. PLoS ONE, 2019, 14, e0212865.	2.5	2
146	Self-guided Multiple Instance Learning for Weakly Supervised Disease Classification and Localization in Chest Radiographs. Lecture Notes in Computer Science, 2021, , 617-634.	1.3	2
147	Clinical MR Biomarkers. Recent Results in Cancer Research, 2020, 216, 719-745.	1.8	2
148	Pancreatic imaging using diffusivity mapping – Influence of sequence technique on qualitative and quantitative analysis. Clinical Imaging, 2022, 83, 33-40.	1.5	2
149	Assessing the influence of the menstrual cycle on APT CEST-MRI in the human breast. Magnetic Resonance Imaging, 2022, 91, 24-31.	1.8	2
150	Discovering Digital Tumor Signatures—Using Latent Code Representations to Manipulate and Classify Liver Lesions. Cancers, 2021, 13, 3108.	3.7	1
151	Dorsal Root Ganglion Morphometric Changes Under Oxaliplatin Treatment. Clinical Neuroradiology, 2021, , 1.	1.9	1
152	Letter to the Editor. European Journal of Radiology, 2016, 85, 1682.	2.6	0
153	Diffusivity mapping of the ovaries: Variability of apparent diffusion and kurtosis variables over the menstrual cycle and influence of oral contraceptives. Magnetic Resonance Imaging, 2021, 80, 50-57.	1.8	0
154	Vesseg. Arteriosclerosis, Thrombosis, and Vascular Biology, 2021, 41, 2516-2522.	2.4	0
155	Critical evaluation of MRI-targeted TRUS-guided transperineal fusion biopsy for detection of prostate cancer Journal of Clinical Oncology, 2013, 31, e16063-e16063.	1.6	0
156	Morphological correlates of oxaliplatin induced peripheral neuropathy assessed by magnetic resonance neurography Journal of Clinical Oncology, 2017, 35, 10092-10092.	1.6	0
157	Quantitative Analysis of DCE and DSC-MRI: From Kinetic Modeling to Deep Learning. RoFo Fortschritte Auf Dem Gebiet Der Rontgenstrahlen Und Der Bildgebenden Verfahren, 2022, , .	1.3	0